Digital Homodyne and Heterodyne Detection for Stationary Bosonic Modes

Ingrid Strandberg,[1] Axel M. Eriksson,[1] Baptiste Royer,[2] Mikael Kervinen,[1,*] and Simone Gasparinetti[1]
[1]*Department of Microtechnology and Nanoscience MC2, Chalmers University of Technology, SE-412 96 Göteborg, Sweden*
[2]*Département de Physique and Institut Quantique, Université de Sherbrooke, Sherbrooke J1K 2R1 Quebec, Canada*

(Received 8 January 2024; revised 20 March 2024; accepted 9 July 2024; published 5 August 2024)

Homo- and heterodyne detection are fundamental techniques for measuring propagating electromagnetic fields. However, applying these techniques to stationary fields confined in cavities poses a challenge. As a way to overcome this challenge, we propose to use repeated indirect measurements of a two-level system interacting with the cavity. We demonstrate numerically that the proposed measurement scheme faithfully reproduces measurement statistics of homo- or heterodyne detection. The scheme can be implemented in various physical architectures, including circuit quantum electrodynamics. Our results pave the way for implementation of quantum algorithms requiring linear detection of stationary modes, including quantum verification protocols.

DOI: 10.1103/PhysRevLett.133.063601

Introduction—Continuous monitoring of quantum states of light has a long history in quantum optics. Direct photon detection [1,2] and homodyne detection [3,4] were used to reveal nonclassical properties of the electromagnetic field already in the 1980s. These methods, along with heterodyne detection, are basic techniques for detecting optical radiation [5,6]. Since the 2000s, with the advent of circuit quantum electrodynamics [7] as a platform for quantum information processing, there has been an increased interest in detecting microwave radiation at the quantum level. While photon number resolving detection of propagating microwave photons is challenging due to their low energy [8], homodyne and heterodyne detection of propagating fields can be performed thanks to the availability of low-noise linear amplifiers [9]. These types of measurements are of interest since they suffice to implement any multimode Gaussian operation in continuous-variable measurement-based quantum computation [10,11], boson sampling [12,13] as well as efficient verification of it [14], and reliable verification of an untrusted state preparation [15,16]. Unfortunately, these types of measurements are not straightforward to perform on confined cavity fields which are important for quantum computing with bosonic modes [17–19].

Information about a cavity field can be obtained by measuring leakage out of the cavity, but since photon loss is an obstacle for bosonic quantum information processing, cavities with a low loss rate are generally desired, which makes monitoring the leaked output inefficient. One way to overcome this problem is to swap the stationary mode with a propagating mode [20], which requires added hardware and tunable couplers which are difficult to engineer. An alternative is to indirectly probe the cavity field. This type of indirect measurement was first performed to measure the photon number inside a cavity by letting Rydberg atoms cross it and measuring the atoms afterward [21]. Similar ideas have subsequently been used in superconducting circuits, where a qubit has not only been used as a probe for measurement of the photon number [22], but also the cavity Wigner function [23–25]. However, to date, highly efficient homo- or heterodyne detection measurements of cavity modes are lacking.

In this Letter, we propose using a sequence of indirect measurements, assisted by an ancillary qubit, to perform a digital version of homodyne and heterodyne detection of a stationary bosonic mode. For this reason, we refer to our measurement protocol as *qubitdyne* detection. We demonstrate by numerical calculations that the qubitdyne protocol reproduces measurement statistics of homodyne and heterodyne detection. The simple interaction Hamiltonian needed to perform qubitdyne measurements can be implemented in a variety of systems: trapped ions and atoms [26,27], nanomechanical oscillators [28], NV centers [29], and superconducting circuits [7].

Repeated indirect measurements setup—Our qubitdyne setup can be described as a realization of a so-called *repeated quantum interactions model* [30,31] or *collision model* [32–34]. This type of model reproduces open quantum system dynamics [30–35], and have been used for investigating systems with complex environments [36–38]. In the general model, a quantum system is in contact

[*]Present address: VTT Technical Research Centre of Finland Ltd. Tietotie 3, Espoo 02150, Finland.

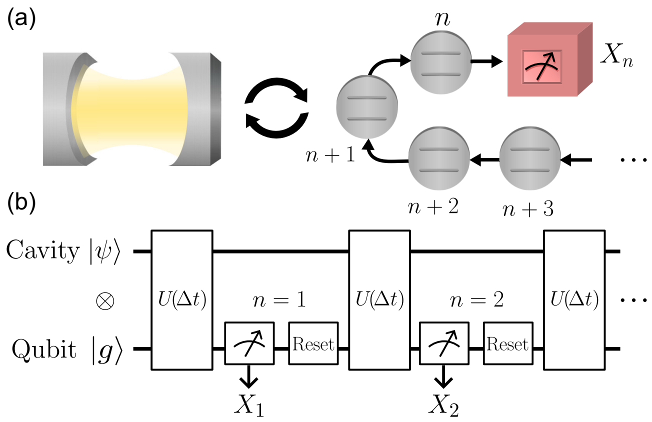

FIG. 1. The system realizing digital homo- and heterodyne detection of a stationary mode. (a) Interaction and subsequent measurement of independent qubits interacting with a cavity, with measurement outcome $X_n = \pm 1$ for the nth qubit. (b) Circuit diagram representation of the procedure. The total system evolves with a unitary operator $U(\Delta t)$ during a time interval Δt, corresponding to a partial SWAP. A projective measurement is performed on the qubit, after which it is reset to its ground state. The process is repeated and a sequence of measurement outcomes $\{X_1, X_2, ..., X_{N_{\text{bit}}}\}$ is obtained.

with an environment represented as a chain of independent smaller systems called probes. The system time evolution is obtained by consecutive interactions with each probe during a short time interval Δt, and after each interaction a measurement is performed on the corresponding probe [39,40]. In our case, the primary system is a long-lived cavity. If the interaction time is sufficiently short and the coupling weak, the probability of transferring more than one photon from the cavity to a probe is negligible, meaning that each probe can be represented as a two-level system, i.e., a qubit [41]. Our setup operates in this regime, illustrated in Fig. 1(a). To simplify the realization of the model, instead of a chain of qubits, we consider a single qubit that is reset to its ground state after each measurement. The quantum circuit realizing our scheme is drawn in Fig. 1(b). The cavity and qubit modes are represented by creation and annihilation operators $a^\dagger$, a and σ_+, σ_-, respectively. With a Jaynes-Cummings coupling between the systems, the unitary evolution for an interaction of time Δt is

$$U = \exp\left(-i\phi_{\text{int}}(a\sigma_+ + a^\dagger\sigma_-)\right), \quad (1)$$

where we define an effective interaction strength $\phi_{\text{int}} = \sqrt{\gamma \Delta t}$ where $\sqrt{\gamma/\Delta t}$ is the coupling strength between the qubit and cavity [42,43]. Since the qubit is always in the ground state before interaction, photons are transferred out of the cavity, corresponding to an effective loss rate $\gamma = \phi_{\text{int}}^2/\Delta t$. The parameter γ is the loss rate for the open systems model in the continuous limit, while it corresponds to a measurement rate in our protocol, representing decay into the measurement apparatus instead of an uncontrolled environment. Each interaction via the unitary (1) can also be regarded as a partial SWAP for small ϕ_{int}, since the operation corresponds to an iSWAP for $\phi_{\text{int}} = \phi_{\text{SWAP}} = \pi/2$.

During the interaction-measurement sequence, the cavity state will evolve stochastically as a quantum trajectory conditioned on the qubit measurement result. Measuring in the σ_x or σ_y basis, or alternating between these, gives rise to diffusive trajectories of the state corresponding to homodyne or heterodyne detection, respectively [37,44], while measuring in the z basis gives rise to quantum jumps corresponding to photodetection. We utilize the model to show that the *measurement record*, by choice of qubit observable, provides the same statistics as quadrature measurements of the cavity.

Qubitdyne: Digital homo- and heterodyne detection—An ideal homodyne detector measures the *generalized quadrature*

$$x_\theta = \frac{1}{\sqrt{2}}(a^\dagger e^{i\theta} + a e^{-i\theta}), \quad (2)$$

which reduces to the ordinary x and p quadratures for $\theta = 0$ and $\theta = \pi/2$, respectively. Analogously to a regular homodyne measurement where the quadrature is determined by the phase reference of a local oscillator, qubitdyne chooses a quadrature by selecting a measurement axis in the xy plane of the qubit Bloch sphere, which is controlled by the phase of the drive pulse that rotates the qubit for measurement in the computational basis. An example of the qubit-cavity correspondence is the direct relation between their expectation values [45]

$$\langle \sigma_- \rangle = -i\sqrt{\gamma \Delta t}\langle a \rangle. \quad (3)$$

We also show that the stochastic difference equation for the qubitdyne signal takes the same form as the stochastic differential equation for the homodyne current (see Sec. II in [45]), establishing a correspondence at the level of individual quantum trajectories. Below we show numerically that the qubitdyne protocol obtains measurement results that are statistically equivalent to homodyne detection. To determine the full probability distribution of measurement outcomes, we produce a large number of trajectories. If $X_n = \pm 1$ is the random variable corresponding to the qubit measurement outcome at step n, the result of one trajectory with N_{bit} qubit measurements is given by the random variable

$$J_{\text{hom}} = \sum_n^{N_{\text{bit}}} f(t_n) X_n, \quad (4)$$

where the digital measurement result is weighted by the function

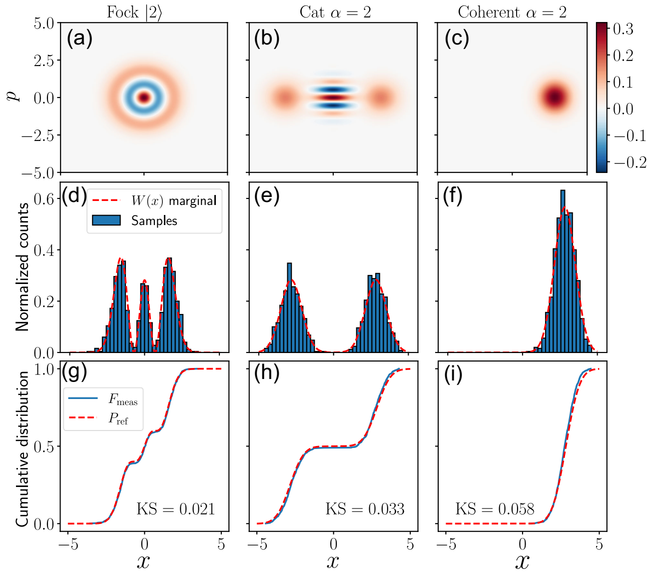

FIG. 2. Simulated qubitdyne measurements corresponding to a homodyne record. Each column corresponds to a unique state. Top row: Ideal Wigner functions. Middle row: Histograms from 1000 measurement rounds, compared to the ideal Wigner marginals (dashed lines). Bottom row: Simulated cumulative distribution functions F_{meas} (solid lines) and ideal distributions P_{ref} (dashed lines). The distance between the two distributions is quantified by the Kolmogorov-Smirnov (KS) statistic. Simulations used interaction strength $\phi_{\text{int}} = 0.1\phi_{\text{SWAP}}$ and $N_{\text{bit}} = 200$ qubit measurements.

$$f(t_n) = \sqrt{\gamma\Delta t/2}\exp(-\gamma t_n/2), \tag{5}$$

at time step $t_n = n\Delta t$. As in ordinary homodyne measurement, the function (5) corresponds to the mode shape used for temporal mode matching of a field leaking into a waveguide with rate γ [69,70].

The probability distribution for homodyne detection is the marginal distribution of the Wigner function along the measured quadrature [5], and we demonstrate that the values J_{hom} of Eq. (4) are sampled from this distribution by simulating N_{trajs} realizations of the stochastic process. As an example, we show simulated measurement statistics for three different states, Fock $|2\rangle$, cat $(|\alpha\rangle + |-\alpha\rangle)/\sqrt{2}$, and coherent $|\alpha\rangle$ states with $\alpha = 2$, whose Wigner functions are displayed in Figs. 2(a)–2(c). Normalized histograms with values calculated as Eq. (4) from $N_{\text{trajs}} = 1000$ simulated measurement rounds with $N_{\text{bit}} = 200$ qubit measurements each are shown in Figs. 2(d)–2(f). As a quantitative measure of how well our digitized homodyne measurement corresponds to an ideal measurement, we use the Kolmogorov-Smirnov (KS) statistic [71,72]. The KS statistic measures the largest vertical distance between the empirical and reference cumulative distribution functions $F_{\text{meas}}(x)$ and $P_{\text{ref}}(x)$:

$$\text{KS} = \max_x |F_{\text{meas}}(x) - P_{\text{ref}}(x)|. \tag{6}$$

The empirically sampled distributions and the ideal distributions calculated from the Wigner marginals, along with the KS statistics, are displayed in Figs. 2(g)–2(h). We also use the fidelity of a state reconstruction as a proxy for the statistical accuracy of the data. Using the reconstruction method from Ref. [73], a fidelity of 0.99 is obtained for all three states with simulated measurements of 10 quadrature angles.

There are two key criteria that need to be met to produce accurate measurement statistics: (i) the qubit excitation probability must be small, and (ii) the cavity must be almost empty by the final measurement. The probability to excite the qubit during an interaction is [45]

$$p_e = \gamma\Delta t\langle a^\dagger a\rangle = \phi_{\text{int}}^2\langle a^\dagger a\rangle, \tag{7}$$

depending not only on the interaction strength but also on the average cavity photon number $\langle a^\dagger a\rangle$. For any given cavity state, the effective interaction strength must be chosen such that the condition

$$p_e \ll 1, \tag{8}$$

is fulfilled. Additionally, the state must be sufficiently extracted from the cavity to obtain complete information on the initial mode. This requirement means that for a given interaction strength, a minimum number of qubit measurements N_{bit} are needed such that $N_{\text{bit}}\phi_{\text{int}}^2 \gg 1$. Using the same cat state as before, again with interaction $\phi_{\text{int}} = 0.1\phi_{\text{SWAP}}$ and $N_{\text{trajs}} = 1000$, Fig. 3 shows the infidelity, KS statistic, and final cavity population for different values of N_{bit}. It can be seen that accurate statistics are only obtained when most of the state has been extracted at the end of a measurement round. In this example, a fidelity of 0.99 is first obtained when the cavity field has reached around 94% vacuum.

Next, we present heterodyne detection, which measures two orthogonal quadratures simultaneously at the cost of additional measurement noise due to Heisenberg's uncertainty principle. Heterodyne measurement statistics is obtained by interleaving σ_y and σ_x measurements. The result of one measurement round with a total of N_{bit} qubit measurements is given by

$$J_{\text{het}} = \sum_{n=1}^{N_{\text{bit}}-1} 2[f(t_n)Y_n + \mathrm{i}f(t_{n+1})X_{n+1}], \tag{9}$$

with the weight function (5), X_n being the outcome of σ_x measurements, and Y_n of σ_y measurements. Two-dimensional histograms of $N_{\text{trajs}} = 10\,000$ measurement rounds with $N_{\text{bit}} = 300$ qubit measurements are shown in the bottom row of Fig. 4 for the state $|2\rangle$, cat $(|\alpha\rangle + |-\alpha\rangle)/\sqrt{2}$, and coherent state $|\alpha\rangle$. These histograms can be compared to the top row of Fig. 4 showing the Q functions corresponding to ideal heterodyne

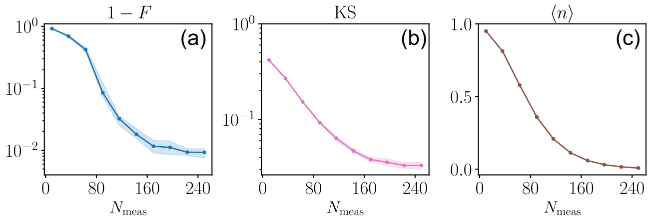

FIG. 3. Measures of statistical accuracy and the final cavity population as a function of the number of qubit measurements N_{bit}, for a cat state of amplitude $\alpha = 2$. (a) Infidelity between the ideal state and the state reconstruction from sampled data. The shaded region indicates the standard deviation of 10 different tomography rounds. (b) Kolmogorov-Smirnov statistic of the sampled data. (c) Cavity population at the end of a measurement round.

measurements. Fidelity of state reconstructions with the sampled data reach at least 0.99.

Effect of finite cavity lifetime—In the optimal scenario without dissipation, qubitdyne measurements approach ideal statistics in the continuous measurement limit, which is attained by reducing ϕ_{int} and increasing N_{bit}. However, in a realistic setting, the cavity dissipation rate κ sets a limit on how many measurements can be made before the cavity state has leaked into the environment. Hence, there will be an optimal interaction strength, depending on the cavity decay rate and initial state.

We determine that the qubitdyne scheme is expected to work with high fidelity for multiphoton states with an average of up to six photons in a cavity with a ratio $1:500$ between the duration T of one measurement step and the cavity lifetime T_1. This ratio is accessible, for instance, in superconducting circuits, assuming a lifetime $T_1 = 1/\kappa = 500$ μs for a 3D

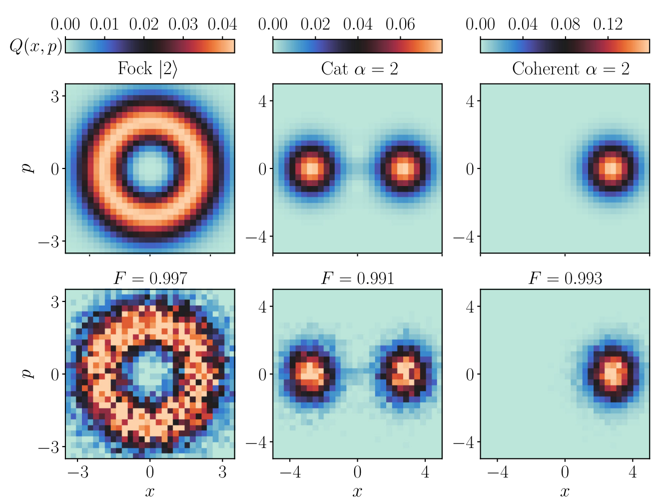

FIG. 4. Qubitdyne measurements corresponding to heterodyne detection. Top row: Ideal discretized Q functions for three different states. Bottom: Heterodyne histograms obtained from alternating σ_x and σ_y measurements, using an interaction strength $\phi_{\mathrm{int}} = 0.1\phi_{\mathrm{SWAP}}$ and $N_{\mathrm{bit}} = 300$ qubit measurements each round. Tomographic fidelity $F > 0.99$ for all three states.

microwave cavity [74] and a total measurement time $T = 1$ μs to complete a single measurement in the sequence, encompassing the duration of a $\Delta t = 300$ ns qubit-cavity interaction [75], qubit measurement [76], and qubit reset [77].

The interplay between cavity decay and measurement strength is visualized in Fig. 5. Figures 5(a) and 5(b) show the infidelity and KS statistic for coherent states with different photon numbers as a function of interaction strength. For each ϕ_{int}, the number of measurements was set such that the cavity was 95% vacuum at the end of each measurement round. Histograms of the simulated measurement statistics at three different interaction strengths for $n = 6$ photons can be seen in Figs. 5(c)–5(d), illustrating three different regimes. First, in panel (c), the interaction is very weak and the field is mostly decaying into the environment, leading to the distribution being mixed with vacuum. In panel (d) an optimal interaction strength is reached. For a stronger interaction in panel (e), the

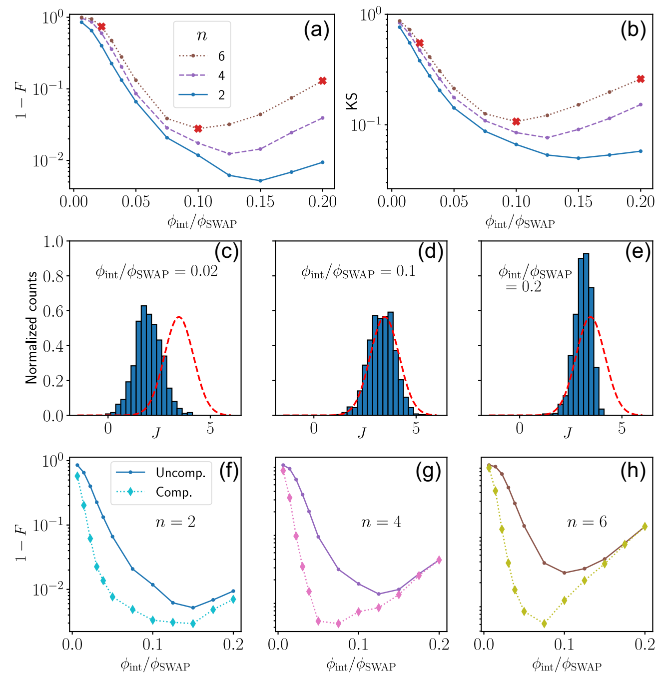

FIG. 5. Homodyne measurement statistics with external cavity dissipation $\kappa = 2$ kHz for coherent states with average photon numbers 2,4, and 6. Interaction time $\Delta t = 300$ ns and measurement time $T = 1$ μs. (a) Tomographic infidelity as a function of interaction strength ϕ_{int}. (b) KS statistic as a function of ϕ_{int}. The markers on the $n = 6$ line indicate interaction strengths for which histograms are visualized in Figs. (c)–(e) Simulated homodyne histograms and corresponding ideal distributions (dashed lines). (c) This interaction strength is too weak and the histogram is shifted towards vacuum. (d) The histogram matches the expected distribution, this is the optimal interaction strength. The corresponding efficiency at this point is $\eta = 0.925$. (e) The interaction is too strong, leading to a distorted histogram. (f)–(h) Infidelities from (a) (solid lines) and noise-compensated infidelities (dashed lines).

distribution is distorted because condition (8) is violated. This condition is necessary for the protocol to be valid, but the effect of a finite cavity lifetime as shown in Fig. 5(c) simply corresponds to a nonideal collection efficiency. With a measurement rate γ and radiative decay rate κ, the photon collection efficiency is

$$\eta = \frac{\gamma}{\gamma + \frac{T}{\Delta t}\kappa}. \tag{10}$$

The ratio $T/\Delta t$ appears since intrinsic loss with rate κ occurs throughout the entire protocol, while the measurement rate γ is only activated during the interaction times Δt. Generally, a reduced efficiency $\eta < 1$ degrades the measured distributions. However, for the purpose of tomographic measurements, it can be compensated for [78] to obtain a reliable state reconstruction. The effect of this compensation is shown in Figs. 5(f)–5(h), where infidelity is reduced in the regime of small ϕ_{int}.

For a coherent state with average photon number $n = 6$, we obtain a maximal collection efficiency $\eta = 0.925$. Assuming an efficiency $\eta_q = 0.98$ from qubit readout error, the total detection efficiency is $\eta_{\mathrm{det}} = \eta_q \eta = 0.91$. This is more than twice the detection efficiency when releasing a multiphoton state of similar size [20].

Enhanced readout speed—As shown in Fig. 3, most photons must be removed from the cavity via the qubit to obtain correct information about the state. The constant coupling ϕ_{int} gives rise to an exponential cavity decay, but the number of measurements needed to empty the cavity is larger for states with higher photon numbers. As seen in Fig. 5, these longer measurement rounds lead to reduced measurement fidelity in the presence of loss. A way to alleviate this problem is to reduce the number of needed measurement by successively increasing the qubit-cavity coupling rate, which allows the cavity to be emptied faster while still keeping the qubit excitation probability low. To obtain accurate measurement statistics for a time-dependent coupling $\phi_{\mathrm{int}}(t)$, we find that the appropriate weight function $f(t)$ has the shape corresponding to the temporal envelope of a single-photon wave packet emitted via such modulation [79–81]. The expression can be obtained by solving the quantum Langevin equation along with the input-output relation, and the resulting expression is given by

$$f(t) = \frac{\phi_{\mathrm{int}}(t)}{\sqrt{2}} \exp\left(-\frac{1}{2\Delta t}\int_0^t \phi_{\mathrm{int}}(t)^2 \mathrm{d}t'\right). \tag{11}$$

As we show in the Supplemental Material [45], the use of a time-dependent coupling strength can reduce the number of measurements by a factor 2, while preserving the measurement fidelity. The analytical relation Eq. (11) enables accurate statistics to be obtained for *any* $\phi_{\mathrm{int}}(t)$, opening the possibility for future optimization of the time-dependent coupling.

Discussion—The measurement scheme presented in this Letter opens the door for quantum information processing protocols that require homo- or heterodyne detection of confined cavity modes. The scheme only requires a beam splitter or SWAP interaction between a two-level system and the bosonic mode of interest, and the ability to repeatedly measure the qubit. This simplicity makes it applicable on a large variety of platforms.

We expect the qubitdyne scheme to perform better than the release of a microwave mode into a transmission line, because the latter measurement is limited by the finite efficiency of the amplification chain used to measure the field quadratures [20], while highly accurate qubit readout is possible even without a quantum-limited amplifier [82].

An alternative version of qubitdyne can be implemented by a phase estimation protocol [83] of the displacement operator, which amounts to a modular quadrature measurement [84] (see Supplemental Material [45]). However, we expect the phase estimation approach to be more sensitive to loss channels than regular qubitdyne because the amount of energy present in the cavity increases with each phase-estimation round, while the cavity is emptied in the presented qubitdyne protocol.

Among possible applications of qubitdyne, we envisage efficient boson sampling verification [14] and quantum state certification [85].

Acknowledgments—S. G. is thankful to Giulia Ferrini, Alessandro Ferraro, and Ulysse Chabaud for useful discussions that initiated this work. I. S. gives thanks to Maryam Khanahmadi for important insights regarding the time-dependent coupling. Simulations were done using QuTiP [86]. This work is supported by the Knut and Alice Wallenberg Foundation via the Wallenberg Centre for Quantum Technology (WACQT). I. S. acknowledges financial support from the European Union via Grant No. 101057977 SPECTRUM. A. E. and S. G. acknowledge funding from the European Union's Horizon Europe Framework Programme (EIC Pathfinder Challenge project Veriqub) under Grant Agreement No. 101114899. B. R. acknowledges funding from the Canada First Research Excellence Fund, the Natural Sciences and Engineering Research Council of Canada (NSERC) as well as the Fonds de Recherche du Québec, Nature et Technologie (FRQNT).

Data availability—The code used to perform numerical simulations in this work is available at [87].

[1] R. Short and L. Mandel, Observation of sub-poissonian photon statistics, Phys. Rev. Lett. **51**, 384 (1983).

[2] J. G. Rarity, P. R. Tapster, and E. Jakeman, Observation of sub-poissonian light in parametric downconversion, Opt. Commun. **62**, 201 (1987).

[3] R. E. Slusher, L. W. Hollberg, B. Yurke, J. C. Mertz, and J. F. Valley, Observation of squeezed states generated by four-wave mixing in an optical cavity, Phys. Rev. Lett. **55**, 2409 (1985).

[4] L.-A. Wu, H. J. Kimble, J. L. Hall, and H. Wu, Generation of squeezed states by parametric down conversion, Phys. Rev. Lett. **57**, 2520 (1986).

[5] U. Leonhardt, *Measuring the Quantum State of Light*, Cambridge Studies in Modern Optics (Cambridge University Press, Cambridge, England, 1997).

[6] H. A. Bachor and T. C. Ralph, *A Guide to Experiments in Quantum Optics*, 2nd ed. (Wiley-VCH Verlag, Weinheim, Germany, 2004).

[7] A. Blais, R.-S. Huang, A. Wallraff, S. M. Girvin, and R. J. Schoelkopf, Cavity quantum electrodynamics for superconducting electrical circuits: An architecture for quantum computation, Phys. Rev. A **69**, 062320 (2004).

[8] R. Dassonneville, R. Assouly, T. Peronnin, P. Rouchon, and B. Huard, Number-resolved photocounter for propagating microwave mode, Phys. Rev. Appl. **14**, 044022 (2020).

[9] C. Eichler, D. Bozyigit, and A. Wallraff, Characterizing quantum microwave radiation and its entanglement with superconducting qubits using linear detectors, Phys. Rev. A **86**, 032106 (2012).

[10] N. C. Menicucci, P. van Loock, M. Gu, C. Weedbrook, T. C. Ralph, and M. A. Nielsen, Universal quantum computation with continuous-variable cluster states, Phys. Rev. Lett. **97**, 110501 (2006).

[11] M. Gu, C. Weedbrook, N. C. Menicucci, T. C. Ralph, and P. van Loock, Quantum computing with continuous-variable clusters, Phys. Rev. A **79**, 062318 (2009).

[12] U. Chabaud, T. Douce, D. Markham, P. van Loock, E. Kashefi, and G. Ferrini, Continuous-variable sampling from photon-added or photon-subtracted squeezed states, Phys. Rev. A **96**, 062307 (2017).

[13] L. Chakhmakhchyan and N. J. Cerf, Boson sampling with Gaussian measurements, Phys. Rev. A **96**, 032326 (2017).

[14] U. Chabaud, F. Grosshans, E. Kashefi, and D. Markham, Efficient verification of boson sampling, Quantum **5**, 578 (2021).

[15] L. Aolita, C. Gogolin, M. Kliesch, and J. Eisert, Reliable quantum certification of photonic state preparations, Nat. Commun. **6**, 1 (2015).

[16] U. Chabaud, T. Douce, F. Grosshans, E. Kashefi, and D. Markham, Building trust for continuous variable quantum states, in *Proceedings of the 15th Conference on the Theory of Quantum Computation, Communication and Cryptography (TQC 2020)*, Leibniz International Proceedings in Informatics (LIPIcs) Vol. 158, edited by S. T. Flammia (Schloss Dagstuhl–Leibniz-Zentrum für Informatik, Dagstuhl, Germany, 2020), pp. 3:1–3:15.

[17] V. V. Sivak, A. Eickbusch, B. Royer, S. Singh, I. Tsioutsios, S. Ganjam, A. Miano, B. L. Brock, A. Z. Ding, L. Frunzio, S. M. Girvin, R. J. Schoelkopf, and M. H. Devoret, Real-time quantum error correction beyond break-even, Nature (London) **616**, 50 (2023).

[18] N. Ofek, A. Petrenko, R. Heeres, P. Reinhold, Z. Leghtas, B. Vlastakis, Y. Liu, L. Frunzio, S. M. Girvin, L. Jiang, M. Mirrahimi, M. H. Devoret, and R. J. Schoelkopf, Extending the lifetime of a quantum bit with error correction in superconducting circuits, Nature (London) **536**, 441 (2016).

[19] A. Joshi, K. Noh, and Y. Y. Gao, Quantum information processing with bosonic qubits in circuit QED, Quantum Sci. Technol. **6**, 033001 (2021).

[20] W. Pfaff, C. J. Axline, L. D. Burkhart, U. Vool, P. Reinhold, L. Frunzio, L. Jiang, M. H. Devoret, and R. J. Schoelkopf, Controlled release of multiphoton quantum states from a microwave cavity memory, Nat. Phys. **13**, 882 (2017).

[21] M. Brune, S. Haroche, V. Lefevre, J. M. Raimond, and N. Zagury, Quantum nondemolition measurement of small photon numbers by Rydberg-atom phase-sensitive detection, Phys. Rev. Lett. **65**, 976 (1990).

[22] D. I. Schuster, A. A. Houck, J. A. Schreier, A. Wallraff, J. M. Gambetta, A. Blais, L. Frunzio, J. Majer, B. Johnson, M. H. Devoret, S. M. Girvin, and R. J. Schoelkopf, Resolving photon number states in a superconducting circuit, Nature (London) **445**, 515 (2007).

[23] K. Banaszek, C. Radzewicz, K. Wódkiewicz, and J. S. Krasiński, Direct measurement of the Wigner function by photon counting, Phys. Rev. A **60**, 674 (1999).

[24] G. Nogues, A. Rauschenbeutel, S. Osnaghi, P. Bertet, M. Brune, J. M. Raimond, S. Haroche, L. G. Lutterbach, and L. Davidovich, Measurement of a negative value for the Wigner function of radiation, Phys. Rev. A **62**, 054101 (2000).

[25] P. Bertet, A. Auffeves, P. Maioli, S. Osnaghi, T. Meunier, M. Brune, J. M. Raimond, and S. Haroche, Direct measurement of the wigner function of a one-photon Fock state in a cavity, Phys. Rev. Lett. **89**, 200402 (2002).

[26] A. Borne, A. Borne, T. E. Northup, R. Blatt, R. Blatt, and B. Dayan, Efficient ion-photon qubit SWAP gate in realistic ion cavity-QED systems without strong coupling, Opt. Express **28**, 11822 (2020).

[27] O. Bechler, A. Borne, S. Rosenblum, G. Guendelman, O. E. Mor, M. Netser, T. Ohana, Z. Aqua, N. Drucker, R. Finkelstein, Y. Lovsky, R. Bruch, D. Gurovich, E. Shafir, and B. Dayan, A passive photon-atom qubit swap operation, Nat. Phys. **14**, 996 (2018).

[28] E. A. Wollack, A. Y. Cleland, R. G. Gruenke, Z. Wang, P. Arrangoiz-Arriola, and A. H. Safavi-Naeini, Quantum state preparation and tomography of entangled mechanical resonators, Nature (London) **604**, 463 (2022).

[29] A.-P. Liu, L.-Y. Cheng, S. Zhang, Y. Zhao, X.-Z. Gao, Y.-H. Chang, and A.-P. Wang, Deterministic controlled-phase gate and SWAP gate with dipole-induced transparency in the weak-coupling regime, Opt. Commun. **379**, 19 (2016).

[30] S. Attal and A. Joye, Weak coupling and continuous limits for repeated quantum interactions, J. Stat. Phys. **126**, 1241 (2007).

[31] L. Bruneau, A. Joye, and M. Merkli, Asymptotics of repeated interaction quantum systems, J. Funct. Anal. **239**, 310 (2006).

[32] F. Ciccarello, Collision models in quantum optics, Quantum Meas. Quantum Metrol. **4**, 53 (2017).

[33] S. Cusumano, Quantum collision models: A beginner guide, Entropy **24**, 1258 (2022).

[34] S. Campbell and B. Vacchini, Collision models in open system dynamics: A versatile tool for deeper insights?, Europhys. Lett. **133**, 60001 (2021).

[35] F. Ciccarello, S. Lorenzo, V. Giovannetti, and G. M. Palma, Quantum collision models: Open system dynamics from repeated interactions, Phys. Rep. **954**, 1 (2022).

[36] A. Dąbrowska, G. Sarbicki, and D. Chruściński, Quantum trajectories for a system interacting with environment in N-photon state, J. Phys. A **52**, 105303 (2019).

[37] S. Daryanoosh, A. Gilchrist, and B. Q. Baragiola, Collisional-model quantum trajectories for entangled-qubit environments, Phys. Rev. A **106**, 022202 (2022).

[38] F. Ciccarello, G. M. Palma, and V. Giovannetti, Collision-model-based approach to non-Markovian quantum dynamics, Phys. Rev. A **87**, 040103(R) (2013).

[39] C. Pellegrini, Markov Chains approximation of jump–diffusion stochastic master equations, Ann. Inst. Henri Poincaré Probab. Stat. **46**, 924 (2010).

[40] Y. Ashida, Continuous observation of quantum systems, in *Quantum Many-Body Physics in Open Systems: Measurement and Strong Correlations* (Springer, Singapore, 2020), pp. 13–28.

[41] T. A. Brun, A simple model of quantum trajectories, Am. J. Phys. **70**, 719 (2002).

[42] K. A. Fischer, R. Trivedi, V. Ramasesh, I. Siddiqi, and J. Vučković, Scattering into one-dimensional waveguides from a coherently-driven quantum-optical system, Quantum **2**, 69 (2018).

[43] J. A. Gross, C. M. Caves, G. J. Milburn, and J. Combes, Qubit models of weak continuous measurements: Markovian conditional and open-system dynamics, Quantum Sci. Technol. **3**, 024005 (2018).

[44] J. Gambetta and H. M. Wiseman, Stochastic simulations of conditional states of partially observed systems, quantum and, J. Opt. B **7**, S250 (2005).

[45] See Supplemental Material at http://link.aps.org/supplemental/10.1103/PhysRevLett.133.063601 for derivations, which includes Refs. [46–68].

[46] L. Bouten, R. van Handel, and M. R. James, A discrete invitation to quantum filtering and feedback control, SIAM Rev. **51**, 239 (2009).

[47] J. Gough and A. Sobolev, Stochastic Schrödinger equations as limit of discrete filtering, Open Syst. Inf. Dyn. **11**, 235 (2004).

[48] A. Barchielli and A. M. Paganoni, Detection theory in quantum optics: Stochastic representation, Quantum Semiclass. Opt. **8**, 133 (1996).

[49] C. Pellegrini, Existence, uniqueness and approximation of a stochastic Schrödinger equation: The diffusive case, Ann. Probab. **36**, 2332 (2008).

[50] M. Bauer and D. Bernard, Convergence of repeated quantum nondemolition measurements and wave-function collapse, Phys. Rev. A **84**, 044103 (2011).

[51] S. Attal, Approximating the Fock space with the toy Fock space, in *Séminaire de Probabilités XXXVI* (Springer, Berlin, Germany, 2004), pp. 477–491.

[52] A. C. R. Belton, Approximation via toy Fock space—the vacuum-adapted viewpoint, in *Quantum Stochastics and Information* (World Scientific, Singapore, 2008), pp. 3–22.

[53] T. Benoist and C. Pellegrini, Large time behavior and convergence rate for quantum filters under standard non demolition conditions, Commun. Math. Phys. **331**, 703 (2014).

[54] M. Bauer, D. Bernard, and T. Benoist, Iterated stochastic measurements, J. Phys. A **45**, 494020 (2012).

[55] F. Klebaner, *Introduction to Stochastic Calculus with Applications* (Imperial College Press, London, 2005).

[56] J. L. Doob, *Stochastic Processes*, Wiley Classics Library (John Wiley & Sons, Nashville, TN, 1990).

[57] M. Bauer, T. Benoist, and D. Bernard, Repeated quantum non-demolition measurements: Convergence and continuous time limit, Ann. Henri Poincaré **14**, 639 (2013).

[58] M. Bauer, D. Bernard, and A. Tilloy, The open quantum Brownian motions, J. Stat. Mech. (2014) P09001.

[59] O. Calin, *An Informal Introduction to Stochastic Calculus with Applications* (World Scientific Publishing, Singapore, 2015).

[60] H. M. Wiseman and G. J. Milburn, Quantum theory of field-quadrature measurements, Phys. Rev. A **47**, 642 (1993).

[61] C. Gardiner and P. Zoller, *Quantum Noise* (Springer, Berlin, Germany, 2004), https://link.springer.com/book/9783540223016.

[62] H. M. Wiseman and G. J. Milburn, *Quantum Measurement and Control* (Cambridge University Press, Cambridge, England, 2009).

[63] M. Hofheinz, H. Wang, M. Ansmann, R. C. Bialczak, E. Lucero, M. Neeley, A. D. O'Connell, D. Sank, J. Wenner, J. M. Martinis, and A. N. Cleland, Synthesizing arbitrary quantum states in a superconducting resonator, Nature (London) **459**, 546 (2009).

[64] S. Zeytinoğlu, M. Pechal, S. Berger, A. A. Abdumalikov, A. Wallraff, and S. Filipp, Microwave-induced amplitude- and phase-tunable qubit-resonator coupling in circuit quantum electrodynamics, Phys. Rev. A **91**, 043846 (2015).

[65] P. Campagne-Ibarcq, E. Zalys-Geller, A. Narla, S. Shankar, P. Reinhold, L. Burkhart, C. Axline, W. Pfaff, L. Frunzio, R. J. Schoelkopf, and M. H. Devoret, Deterministic remote entanglement of superconducting circuits through microwave two-photon transitions, Phys. Rev. Lett. **120**, 200501 (2018).

[66] C. Zhou, P. Lu, M. Praquin, T.-C. Chien, R. Kaufman, X. Cao, M. Xia, R. S. K. Mong, W. Pfaff, D. Pekker, and M. Hatridge, Realizing all-to-all couplings among detachable quantum modules using a microwave quantum state router, npj Quantum Inf. **9**, 54 (2023).

[67] S. Gasparinetti, S. Berger, A. A. Abdumalikov, M. Pechal, S. Filipp, and A. J. Wallraff, Measurement of a vacuum-induced geometric phase, Sci. Adv. **2**, e1501732 (2016).

[68] A. Eickbusch, V. Sivak, A. Z. Ding, S. S. Elder, S. R. Jha, J. Venkatraman, B. Royer, S. M. Girvin, R. J. Schoelkopf, and M. H. Devoret, Fast universal control of an oscillator with weak dispersive coupling to a qubit, Nat. Phys. **18**, 1464 (2022).

[69] G. J. Milburn and S. Basiri-Esfahani, Quantum optics with one or two photons, Proc. R. Soc. A **471**, 20150208 (2015).

[70] N. D. Pozza, H. M. Wiseman, and E. H. Huntington, Deterministic preparation of superpositions of vacuum plus one photon by adaptive homodyne detection: Experimental considerations, New J. Phys. **17**, 013047 (2015).

[71] W. J. Conover, Statistics of the Kolmogorov-Smirnov type, in *Practical Nonparametric Statistics*, 3rd ed., Wiley Series in Probability and Statistics (Wiley, New York, 1998).

[72] F. J. Massey, The Kolmogorov-Smirnov test for goodness of fit, J. Am. Stat. Assoc. **46**, 68 (1951).

[73] I. Strandberg, Simple, reliable, and noise-resilient continuous-variable quantum state tomography with convex optimization, Phys. Rev. Appl. **18**, 044041 (2022).

[74] M. Kudra, M. Kervinen, I. Strandberg, S. Ahmed, M. Scigliuzzo, A. Osman, D. P. Lozano, M. O. Tholén, R. Borgani, D. B. Haviland, G. Ferrini, J. Bylander, A. F. Kockum, F. Quijandría, P. Delsing, and S. Gasparinetti, Robust preparation of Wigner-negative states with optimized SNAP-displacement sequences, PRX Quantum **3**, 030301 (2022).

[75] M. Kudra, T. Abad, M. Kervinen, A. M. Eriksson, F. Quijandría, P. Delsing, and S. Gasparinetti, Experimental realization of deterministic and selective photon addition in a bosonic mode assisted by an ancillary qubit, arXiv:2212.12079.

[76] T. Walter, P. Kurpiers, S. Gasparinetti, P. Magnard, A. Potočnik, Y. Salathé, M. Pechal, M. Mondal, M. Oppliger, C. Eichler *et al.*, Rapid high-fidelity single-shot dispersive readout of superconducting qubits, Phys. Rev. Appl. **7**, 054020 (2017).

[77] P. Magnard, P. Kurpiers, B. Royer, T. Walter, J.-C. Besse, S. Gasparinetti, M. Pechal, J. Heinsoo, S. Storz, A. Blais *et al.*, Fast and unconditional all-microwave reset of a superconducting qubit, Phys. Rev. Lett. **121**, 060502 (2018).

[78] G. M. D'Ariano and C. Macchiavello, Loss-error compensation in quantum-state measurements, Phys. Rev. A **57**, 3131 (1998).

[79] J. E. Gough and G. Zhang, Generating nonclassical quantum input field states with modulating filters, Eur. Phys. J. Quantum Technol. **2**, 1 (2015).

[80] W.-L. Li, G. Zhang, and R.-B. Wu, On the control of flying qubits, Automatica **143**, 110338 (2022).

[81] K. M. Gheri, K. Ellinger, T. Pellizzari, and P. Zoller, Photon-wavepackets as flying quantum bits, Fortschr. Phys. **46**, 401 (1998).

[82] L. Chen *et al.*, Transmon qubit readout fidelity at the threshold for quantum error correction without a quantum-limited amplifier, npj Quantum Inf. **9**, 1 (2023).

[83] M. A. Nielsen and I. L. Chuang, *Quantum Computation and Quantum Information: 10th Anniversary Edition* (Cambridge University Press, Cambridge, England, 2010).

[84] B. M. Terhal and D. Weigand, Encoding a qubit into a cavity mode in circuit QED using phase estimation, Phys. Rev. A **93**, 012315 (2016).

[85] U. Chabaud, G. Roeland, M. Walschaers, F. Grosshans, V. Parigi, D. Markham, and N. Treps, Certification of non-Gaussian states with operational measurements, PRX Quantum **2**, 020333 (2021).

[86] J. R. Johansson, P. D. Nation, and F. Nori, QuTiP 2: A Python framework for the dynamics of open quantum systems, Comput. Phys. Commun. **184**, 1234 (2013).

[87] I. Strandberg, S. Gasparinetti, and B. Royer, Qubitdyne simulation code, 10.5281/zenodo.10412700 (2023), also on GitHub.